Raman spectroscopy and lattice-dynamical calculations of Sc_{3}CrO_{6} single crystals

N. D. Todorov, M. V. Abrashev, S. C. Russev, V. Marinova, R. P. Nikolova, and B. L. Shivachev

Raman spectroscopy and lattice-dynamical calculations of Sc_3CrO_6 single crystals

N. D. Todorov,* M. V. Abrashev, and S. C. Russev

Faculty of Physics, University of Sofia, BG-1164 Sofia, Bulgaria

V. Marinova

Institute for Optical Materials and Technologies, Bulgarian Academy of Sciences, BG-1113 Sofia, Bulgaria

R. P. Nikolova and B. L. Shivachev

Institute for Mineralogy and Crystallography, Bulgarian Academy of Sciences, BG-1113 Sofia, Bulgaria

(Dated: March 27, 2012)

Single crystals of Sc_3CrO_6 were grown by high temperature solution growth method. They were studied using x-ray single crystal diffractometry, scanning electron microscopy (SEM) with x-ray microprobe analysis and micro-Raman spectroscopy. The crystal structure was refined as rhombohedral one with space group $R\bar{3}$, which confirms that it belongs to the Mg_3TeO_6 - structural type family. In the polarized Raman spectra collected at room temperature all $9A_g + 9E_g$ Raman-allowed phonon modes were observed. The experimentally determined frequencies are compared to the results of lattice-dynamical calculations (LDC) using a shell model. The Raman spectra, obtained with increasing temperature up to $600°$ C, do not provide direct indication for structural phase transition. The decrease with increasing temperature of the relative intensity of five A_g lines compared to the rest ones, however, suggests a possible structural phase transition from $R\bar{3}$ to $R\bar{3}c$ above the investigated temperature region.

I. INTRODUCTION

The detailed study of the phase diagrams A_2O_3-B_2O_3 (A and B - rare earths or transition metals) often leads to identification of new ternary oxides.[1] Although, the Sc_2O_3-B_2O_3 phase diagram is poorly investigated, it is known, that under high pressure $ScAlO_3$[2] and $ScCrO_3$[3] perovskites (with GdFeO$_3$ - type, *Pnma* structure) can be obtained in the Sc_2O_3-Al_2O_3 and Sc_2O_3-Cr_2O_3 systems, respectively. At ambient pressure the compound Sc_3AlO_6, which belong to the Mg_3TeO_6 structural type[4–6] could be synthesized.[7] Due to the difference in the structures of Sc_2O_3 (bixbyite type) and Cr_2O_3 (corundum type), it is reasonable to expect in the Sc_2O_3-Cr_2O_3 system existence of new ternary compound, Sc_3CrO_6[1], instead of the solid solution $Sc_{2-x}Cr_xO_3$.

The mixed transition metal - rare earth oxides are interesting, because changing the temperature and pressure complex structural[8] and magnetic[9,10] phase diagrams can be observed. On the other side they were extensively studied because of their broad technological significance. They can be used for low-temperature synthesis of ceramics, as phase stabilizers[11] as well as scintillator materials in nuclear engineering.[12]

We have successfully grown single crystals of Sc_3CrO_6 from Sc_2O_3-Cr_2O_3 melt at ambient pressure. The crystal structure was determined as rhombohedral $R\bar{3}$ (Mg_3TeO_6 structural type). From appropriately chosen crystal faces polarized Raman spectra were collected, which allow us to determine the symmetry of the lines observed. All eighteen Raman-allowed lines were observed and their symmetry was identified. Performing lattice-dynamical calculations and comparing the calculated to the experimental frequencies, the lines were assigned to definite atomic vibrations. Additionally, we have collected Raman spectra at high temperatures up to $600°$ C. The change of the intensity of some lines leads to the conclusion that probably the structure undergoes structural phase transition to $R\bar{3}c$ at higher temperatures above the investigated temperature region.

II. EXPERIMENT

Sc_3CrO_6 crystals were grown by the high temperature solution growth method in Pt crucible. We used Sc_2O_3 of 99.99%, Cr_2O_3 of 99.995%, and PbF_2 and KF of 99.999% purity as starting materials. Solid phase synthesis of Sc_3CrO_6 powder was performed at $1100°$ C in an oxygen atmosphere for 48 h. The complete reaction between the starting materials was controlled by x-ray powder diffractometry. As solvent we used a mixture of PbF_2 and KF in 1 : 4 ratio. The Sc_3CrO_6 to solvent ratio varied from 1 : 7 to 1 : 10. 600 g of this mixture were quasi-hermetically closed in the crucible with a cover in order to prevent the evaporation of PbF_2 which has a high vapor pressure at the growth process temperature. The temperature was increased at a rate of $50°$ C/h to $1150°$ C. To completely dissolve the components of the materials and to achieve a homogeneous solution, the temperature of $1150°$ C was maintained for 48 h and then subsequently lowered at a rate of $1°$ C/h to $900°$ C. At this temperature the crucible was taken out of the oven, the cover was drilled through and the solvent was poured out. The obtained crystals remain on the bottom and the walls of the crucible.

Figure 1 (a) shows the Sc_3CrO_6 single crystals visualized using scanning electron microscope (SEM; Tescan LYRA) equipped with energy-dispersive x-ray spectrometer (EDX; Bruker). The crystals look quasi-cubic with the largest crystal surfaces being of {100}, {110}, and {111} type. The Sc : Cr atomic ratio was determined by EDX as 3.31 : 1 which corresponds to non-
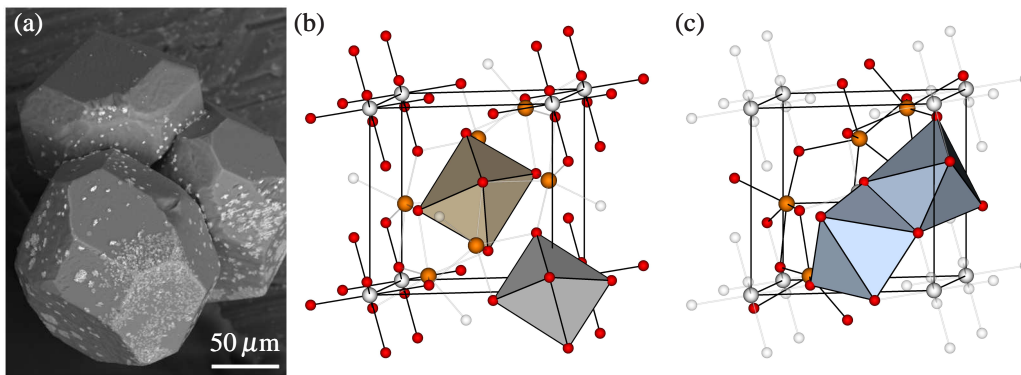

FIG. 1. (Color online) A photo of set of Sc_3CrO_6 single crystals as grown (before cleaning) obtained by scanning electron microscopy - (a). The three types of crystal surfaces, the quasi-cubic {100}, {110}, and {111} ones, are clearly seen. Rhombohedral unit cell of Sc_3CrO_6: (b) the two different $Cr1O_6$ and $(Cr,Sc)2O_6$ octahedra and (c) the edge shared $Sc1O_6$ octahedra are drawn.

stoichiometric compound with chemical content $Sc_6Cr_1Cr_{1-x}Sc_xO_{12}$, $x = 0.08$ (assuming that only Cr2 position is partially occupied by Sc, as discussed further in the text).

The crystallographic characterization of as-grown Sc_3CrO_6 was carried out by x-ray single crystal diffractometry. A single crystal was mounted on a glass capillary and diffraction data were collected at room temperature by ω-scan technique, on an

Agilent Diffraction SuperNova Dual four-circle diffractometer equipped with Atlas CCD detector. A mirror-monochromatized Mo Kα radiation from micro-focus source was used ($\lambda = 0.7107$ Å). The determination of the cell parameters, data integration, scaling and absorption correction were carried out using the CrysAlisPro program package.[13] The structure was solved by direct methods (SHELXS-97)[14] and refined by full-matrix least-square procedures on F^2. The results are listed in Table I.[15]

TABLE I. Structural data of Sc_3CrO_6: atomic labels, Wyckoff notation, occupancy and atomic positions are tabulated. The space group of the crystal is refined as $R\bar{3}$ (# 148), $Z = 2$, $a = 6.1188$ Å, $\alpha = 91.97°$ (rhombohedral cell).

Atom	Wyckoff notation	Occupancy	x	y	z
Cr1	$1a$	1.00	0	0	0
Cr2	$1b$	0.74	1/2	1/2	1/2
Sc2	$1b$	0.26	1/2	1/2	1/2
Sc1	$6f$	1.00	0.24661	0.42868	−0.06275
O1	$6f$	1.00	0.19058	0.42498	−0.41450
O2	$6f$	1.00	0.30779	0.09363	−0.03821

| | | Interatomic distances. | | | |

Pair	Length (Å)	Pair	Length (Å)	Pair	Length (Å)
Cr1-O1	1.974	Sc-O1	2.055	Sc-O2	2.099
Cr2-O2	2.023	Sc-O1	2.167	Sc-O2	2.106
$\langle$Sc-O$\rangle$	2.125	Sc-O1	2.185	Sc-O2	2.139

The Raman measurements were carried out using micro-Raman spectrometer LabRAM HR800 Visible. At room temperature an objective $\times 100$ was used both to focus the incident laser beam and to collect the scattered light. To check the presence of resonance effects in the Raman spectra, He-Ne (633 nm) and Ar^+ (514 and 458 nm) lasers were used as excitation sources. For the high temperature measurements a heating stage Linkam TH600 and a long working distance $\times 50$ objective were used.

To find out the origin of the Raman lines we performed shell-model lattice-dynamical calculations (LDC) based on interatomic potentials represented as a sum of long-range Coulomb potential and short-range potential in the Born-Mayer-Buckingham form $U_{\text{short-range}} = A\exp(-r/\rho) - C/r^6$.

TABLE II. Parameters of the potentials of the shell-shell and core-shell interactions used for LDC. The values for Cr and O are taken from Ref. 16.

Ion	Z ($|e|$)	Y ($|e|$)	k ($e^2\text{Å}^3$)	Ionic pair	A (eV)	ρ (Å)	C ($eV\text{Å}^6$)
Sc	2.97			Sc-O	1326.5	0.3211	0.000
Cr	0.30	2.80	49.5	Cr-O	1763.0	0.2960	0.000
O	0.82	−2.82	96.2	O-O	22764.3	0.1490	27.879

In this model an ion is divided into a core with charge Z, which represent the nucleus and the inner electrons of the ion. As the core has all of the ion mass, the valence electrons are represented by a massless shell with charge Y. The ionic polarizability α is accounted as the interaction between the core and the shell. If this interaction is modeled with a harmonic spring of force constant k, then the polarizability is given by $\alpha = Y^2/k$. The calculations were carried out using the GULP code[17]. The parameters Z, Y, k, A, ρ and C are listed in Table II.

III. DISCUSSION

The crystal structure of Sc_3CrO_6, as determined by x-ray single crystal diffractometry, has space group $R\bar{3}$, [# 148, $Z = 2$, see Fig. 1 (b) and (c)]. Due to the smaller Cr1-O1 distance compared to the Cr2-O2 one, it is plausible to propose that as in the case of Sc_3AlO_6[7] the $1a$ Wyckoff position (in the rhombohedral cell) is occupied by Cr1 atoms, whereas the $1b$ Wyckoff position is occupied randomly by Cr2 and Sc2. This is confirmed by the structure refinement where 74% of the $1b$ position is occupied by Cr2 and 26% by Sc2 atoms. The atoms at these positions do no take part in Raman-active vibrations. The rest Sc1 atoms and the O1 and O2 oxygen atoms occupy general $6f$ Wyckoff positions, so the total number of the Raman-active modes is $9A_g + 9E_g$[18] (see Table III). The Raman tensors of these modes in an orthogonal basis with two axes coinciding with two of the axes of the

TABLE III. Wyckoff position and site symmetry of the atoms in the rhombohedral unit cell of Sc_3CrO_6. The irreducible representations of the Γ-point phonon modes are $\Gamma_{Total} = 9A_g + 9E_g + 11A_u + 11E_u$.

Atom	Wyckoff notation	Site symmetry	Irreducible representations
Cr1	1a	S_6	$A_u + E_u$
(Cr,Sc)2	1b	S_6	$A_u + E_u$
Sc1	6f	C_1	$3A_g + 3A_u + 3E_g + 3E_u$
O1	6f	C_1	$3A_g + 3A_u + 3E_g + 3E_u$
O2	6f	C_1	$3A_g + 3A_u + 3E_g + 3E_u$

hexagonal basis of $R\bar{3}$ are:

$$A_g = \begin{pmatrix} a & 0 & 0 \\ 0 & a & 0 \\ 0 & 0 & b \end{pmatrix}, \ E_g^{(1)} = \begin{pmatrix} c & d & e \\ d & -c & f \\ e & f & 0 \end{pmatrix} \text{ and}$$

$$E_g^{(2)} = \begin{pmatrix} d & -c & -f \\ -c & -d & e \\ -f & e & 0 \end{pmatrix}.$$

At first glance it looks easy to distinguish the lines in the Raman spectra with either A_g or E_g symmetry. However, all polarized Raman spectra (in parallel or crossed polarization), collected from the easiest to recognize $\{100\}_{cub}$ crystal surfaces contain eighteen lines with rather arbitrary intensity, depending on the orientation of the polarization of the incident laser beam (parallel or at 45 deg) according to the edge of the surface. The separation of the lines by symmetry into two groups can be done from the polarized Raman spectra, collected in some special geometrical configurations. If x, y and z is a orthogonal basis, where z is
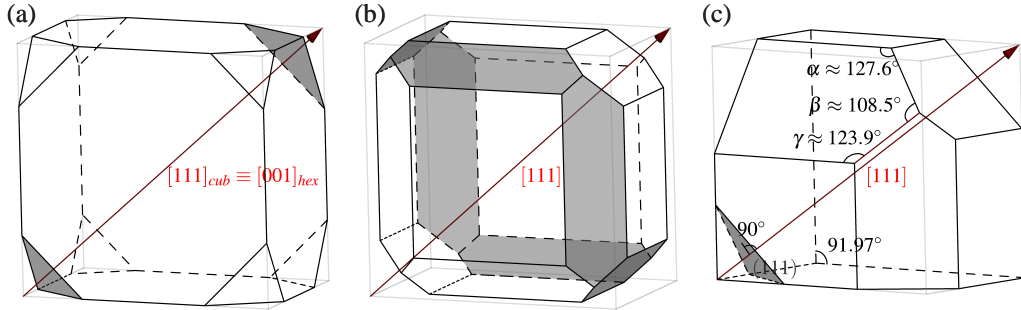

FIG. 2. (Color online) (a) Quasi-cubic crystal with eight $\{111\}_{cub}$ surfaces. Only two of them (in grey) coincide with the $\{001\}_{hex}$ ones. (b) Quasi-cubic crystal with twelve $\{110\}_{cub}$ surfaces. Only six of them (in grey) contain the $[001]_{hex}$ direction. (c) A sketch of the real rhombohedral Sc_3CrO_6 crystal with three $\{110\}_{cub}$ surfaces. The calculated angles between the edges of a $\{110\}_{cub}$ surface, containing the $[001]_{hex}$ direction, are shown.

parallel to the z_{hex} axis and x and y are two arbitrary directions in $(001)_{hex}$ plane, then in zz spectrum only lines with A_g symmetry can be seen, whereas in zx spectrum only E_g lines are allowed. These spectra can be obtained from any $(mn0)_{hex}$ plane. In the Raman spectra, collected from a $(001)_{hex}$ plane, the E_g lines must be seen with equal intensity in xx and xy polarizations. In contrast, the A_g lines can be seen only in xx polarization.

It is not easy to recognize these types of planes among the crystal surfaces of the quasi-cubic single crystals. From Fig. 2 it can be seen that among the eight $\{111\}_{cub}$ crystal surfaces only two are $(001)_{hex}$ ones, whereas six out of the twelve $\{110\}_{cub}$ crystal surfaces have an edge, parallel to the $[001]_{hex}$ direction. Moreover, the $\{110\}_{cub}$ crystal surface edge, parallel to the $[001]_{hex}$ direction, can be recognized by the specific angles between it and adjacent surface edges [see Fig. 2 (c)]. Rolling the single crystals, we have succeed to find the surfaces with the appropriate orientations. The Raman spectra, collected from these two types of surfaces are shown in Fig. 3. In zz spectrum eight out of the nine allowed A_g lines are seen at 222, 259, 331, 405, 445, 458, 668, and 698 cm.$^{-1}$ Their intensity in this spectrum is proportional to the square of the b component of the Raman tensor. The ninth A_g line can be seen only in xx and AA spectra at 343 cm.$^{-1}$ In these spectra the intensity of the A_g lines is proportional to the square of the a component of the Raman tensor. In zx spectrum only E_g lines are allowed and they are positioned at 243, 277, 319, 372, 393, 426, 519, 573, and 638 cm.$^{-1}$
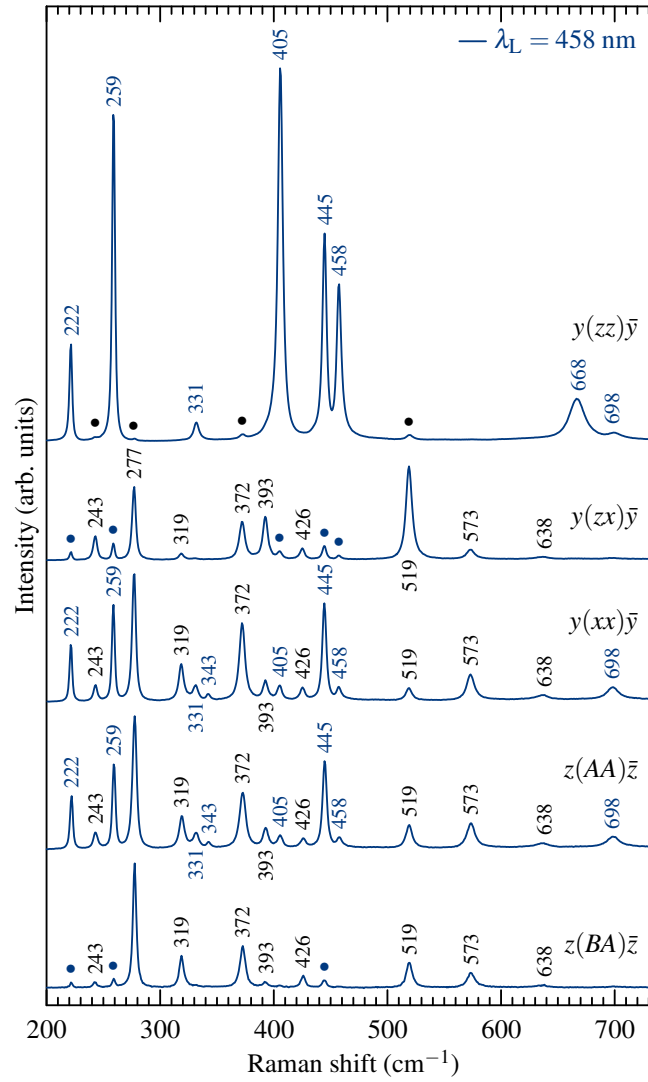
FIG. 3. (Color online) Polarized Raman spectra of Sc$_3$CrO$_6$, collected from $(mn0)_{hex}$ and $(001)_{hex}$ planes with $\lambda_L = 458$ nm excitation at room temperature. The lines, indicated with wavenumber (in cm^{-1} colored in blue for the A_g and black for the E_g ones), are allowed for the corresponding geometrical configuration. The lines, marked with filled circles, are forbidden for the given configuration.

TABLE IV. The frequencies of the $9A_g + 9E_g$ modes, experimentally observed in the Raman spectra and calculated by LDC.

Mode	Expt. (cm^{-1})	Calc. (cm^{-1})	Mode	Expt. (cm^{-1})	Calc. (cm^{-1})
$A_g(1)$	222	222	$E_g(1)$	243	225
$A_g(2)$	259	248	$E_g(2)$	277	274
$A_g(3)$	331	316	$E_g(3)$	319	296
$A_g(4)$	343	328	$E_g(4)$	372	335
$A_g(5)$	405	430	$E_g(5)$	393	407
$A_g(6)$	445	466	$E_g(6)$	426	423
$A_g(7)$	458	520	$E_g(7)$	519	518
$A_g(8)$	668	669	$E_g(8)$	573	578
$A_g(9)$	698	697	$E_g(9)$	638	646

The E_g intensity in the zx spectrum is proportional to $e^2 + f^2$ (e and f are components of the E_g Raman tensor). In the AA and BA [A and B are two arbitrary perpendicular directions in the $(001)_{hex}$ plane] spectra the E_g lines must be of equal intensity,

proportional to $c^2 + d^2$ (c and d are components of the E_g Raman tensor). As it is seen from the *AA* and *BA* spectra, nine lines obey this rule at the same positions as the lines observed in *zx* spectrum. The results are summarized in Table IV. Additionally from the spectra, shown in Fig. 3, except the symmetry of the eighteen Raman-allowed lines, also the ratio of the values of the non-zero components of the Raman tensors of the allowed lines can be evaluated.
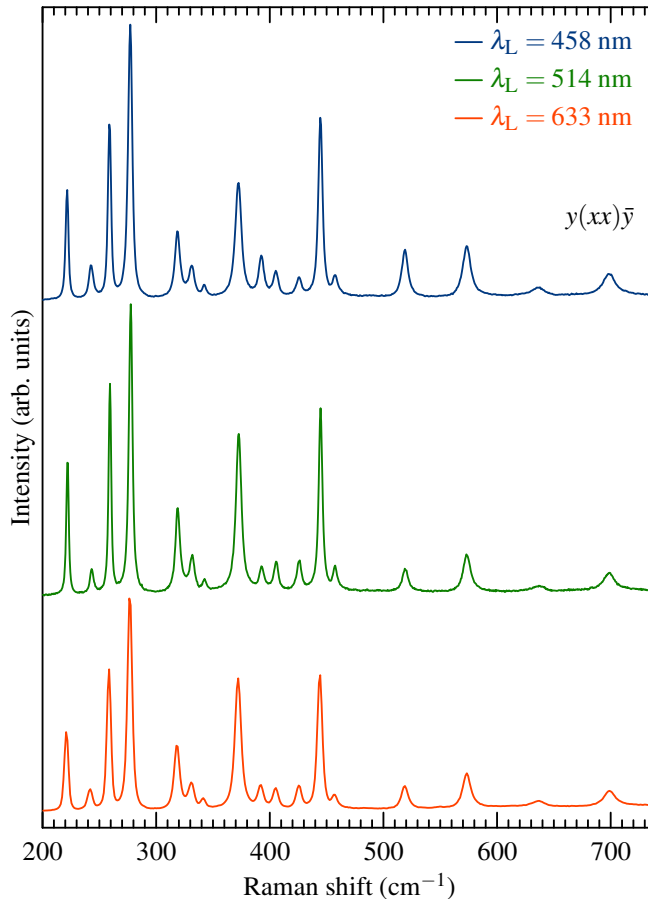

FIG. 4. (Color online) $y(xx)\bar{y}$ polarized Raman spectra of Sc_3CrO_6, obtained with three different laser lines 458, 514, and 633 nm.

In Fig. 4 are shown the $y(xx)\bar{y}$ polarized Raman spectra obtained with three different laser lines. It is seen that the relative intensity of all lines observed practically does not depend on the energy of the exciting photons. It means that there are no resonance effects influencing on the intensity of the lines. Therefore, if an intensity change is observed (e.g. with the temperature, see below), it is most likely connected to some special features of the crystal structure.

Fig. 5 shows non-polarized Raman spectra obtained from $(mn0)_{hex}$ surface with 514 nm laser excitation in the temperature range $20 - 600°$ C. The changes of the parameters of the Raman lines are monotonous, a sign for a lack of structural phase transition in this temperature region. However, the careful comparison of the spectra shows that the intensity of five A_g lines (marked with empty circles in Fig. 5) decreases with increasing temperature. We fitted the intensities of all lines in the spectra at different temperatures. Plot of the normalized ratio of the intensity of each of these five A_g lines and the intensity of the nearest to it non-vanishing line, versus the temperature T is shown in Fig. 6. It is seen that this ratio decreases with the temperature monotonically. Extrapolating this behavior to higher temperatures, it appears that at $T \approx 1000°$ C these five lines must disappear in the Raman spectra. To explain such behavior we look for arguments in specific features of the crystal structure. Generally speaking, the symmetry of the real rhombohedral structure ($\alpha = 91.97°$) can be increased in two ways: (a) if the $Cr1O_6$ and $(Cr,Sc)2O_6$ octahedra become identical or (b) the structure becomes cubic. The rhombohedral structure with identical octahedra has $R\bar{3}c$ symmetry, the cubic structure with different octahedra has $Pm\bar{3}$ symmetry, and the cubic structure with identical octahedra has $Pm\bar{3}n$ symmetry.

The analysis of vibrational modes in the real structure could be done in different ways. Due to the fact that the structure contains different types of octahedra (CrO_6 and ScO_6) with different length of the Cr-O and Sc-O bonds, a molecular approach for description of the structure and analysis of the vibrational modes can be applied. This approach was used to assign the modes observed in the isostructural Mg_3TeO_6[19]. In Ref. 19, however, it has been plausible to use it because of the large charge difference of the Mg^{2+} and Te^{6+} ions. In that case the crystal structure can be regarded as containing isolated TeO_6 octahedra

and Mg ions between them. If so, the type of vibrations for the high frequency modes can be determined as their shape will be typical one for an isolated TeO_6 octahedron (XY_6 molecule, see Ref. [20]).
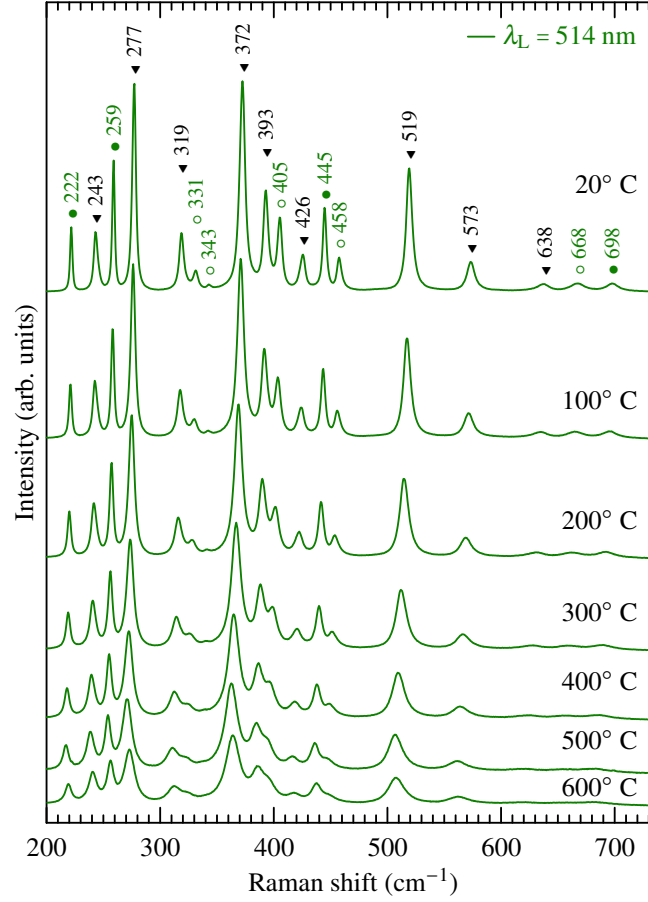

FIG. 5. (Color online) Non-polarized Raman spectra obtained from $(mn0)_{hex}$ surface in the temperature range $20 - 600°$ C. The E_g lines are marked with triangles and the A_g lines are marked with circles. Upon the increase of the temperature, the five A_g lines, which intensity decreases in comparison to the intensity of the other lines, are marked with empty circles.

TABLE V: Correlation between vibrational modes of a XY_6 molecule (CrO_6 octahedron) and modes in hypothetical $Pm\bar{3}n$, $R\bar{3}c$ and the real $R\bar{3}$ crystal structure of Sc_3CrO_6.

	Symmetry of free unit	Site symmetry in O_h^3	Crystal symmetry	Crystal symmetry	Crystal symmetry
CrO_6 octahedra	O_h	T_h	O_h^3 ($Pm\bar{3}n$)	D_{3d}^6 ($R\bar{3}c$)	$C_{3i}^2 \equiv S_6^2$ ($R\bar{3}$)
	A_{1g} (ν_1)	A_g	$A_{1g}+A_{2g}$	$A_{1g}+A_{2g}$	$2A_g$
	E_g (ν_2)	E_g	$2E_g$	$2E_g$	$2E_g$
	F_{2g} (ν_5)	F_g	$F_{1g}+F_{2g}$	$A_{2g}+E_g+A_{1g}+E_g$	$2A_g+2E_g$
	F_{1u} (ν_3)	F_u	$F_{1u}+F_{2u}$	$A_{2u}+E_u+A_{1u}+E_u$	$2A_u+2E_u$
	F_{1u} (ν_4)	F_u	$F_{1u}+F_{2u}$	$A_{2u}+E_u+A_{1u}+E_u$	$2A_u+2E_u$
	F_{2u} (ν_6)	F_u	$F_{1u}+F_{2u}$	$A_{2u}+E_u+A_{1u}+E_u$	$2A_u+2E_u$
	F_{1g} (rot)	F_g	$F_{1g}+F_{2g}$	$A_{2g}+E_g+A_{1g}+E_g$	$2A_g+2E_g$
	F_{1u} (tr)	F_u	$F_{1u}+F_{2u}$	$A_{2u}+E_u+A_{1u}+E_u$	$2A_u+2E_u$
Sc atoms			O_h^3 ($Pm\bar{3}n$)	D_{3d}^6 ($R\bar{3}c$)	$C_{3i}^2 \equiv S_6^2$ ($R\bar{3}$)
			A_{2g}	A_{2g}	A_g
			E_g	E_g	E_g
			F_{1g}	$A_{2g}+E_g$	A_g+E_g
			$2F_{1u}$	$2A_{2u}+2E_u$	$2A_u+2E_u$

TABLE V: (*Continued*).

	F_{2g} F_{2u}	$A_{1g} + E_g$ $A_{1u} + E_u$	$A_g + E_g$ $A_u + E_u$
O_h^3 ($Pm\bar{3}n$)	$\Gamma_{\text{Total}} = A_{1g} + 2A_{2g} + 3E_g + 3F_{1g} + 3F_{2g} + 6F_{1u} + 5F_{2u}$		
D_{3d}^6 ($R\bar{3}c$)	$\Gamma_{\text{Total}} = 4A_{1g} + 5A_{2g} + 9E_g + 5A_{1u} + 6A_{2u}$		
$C_{3i}^2 \equiv S_6^2$ ($R\bar{3}$)	$\Gamma_{\text{Total}} = 9A_g + 9E_g + 11A_u + 11E_u$		

The results using the molecular approach for Sc_3CrO_6 are given in Table V. A single XY_6 molecule has six internal modes and one triply degenerated rotational mode. Constructing a cubic $Pm\bar{3}n$ crystal structure with two identical XY_6 molecules in the primitive cell, the number of Γ-point modes for this structure are two times larger than the number of the octahedral modes due to the presence of Davydov's pairs (pair of modes that are identical for each octahedron but differ by the phase of vibration for the two octahedra, see Ref. [21] and [22]). Lowering the symmetry of this hypothetical cubic crystal to rhombohedral $R\bar{3}c$ one, the triply degenerated modes split into pairs of one non-degenerated and one double-degenerated mode. This approach predicts that some of the vibrational modes in the real Sc_3CrO_6 structure should be grouped into sets of two or four modes with close frequency (see the last column of Table V). To obtain all vibrational modes in the real Sc_3CrO_6, the modes originating from Sc atoms, have to be accounted for, too.
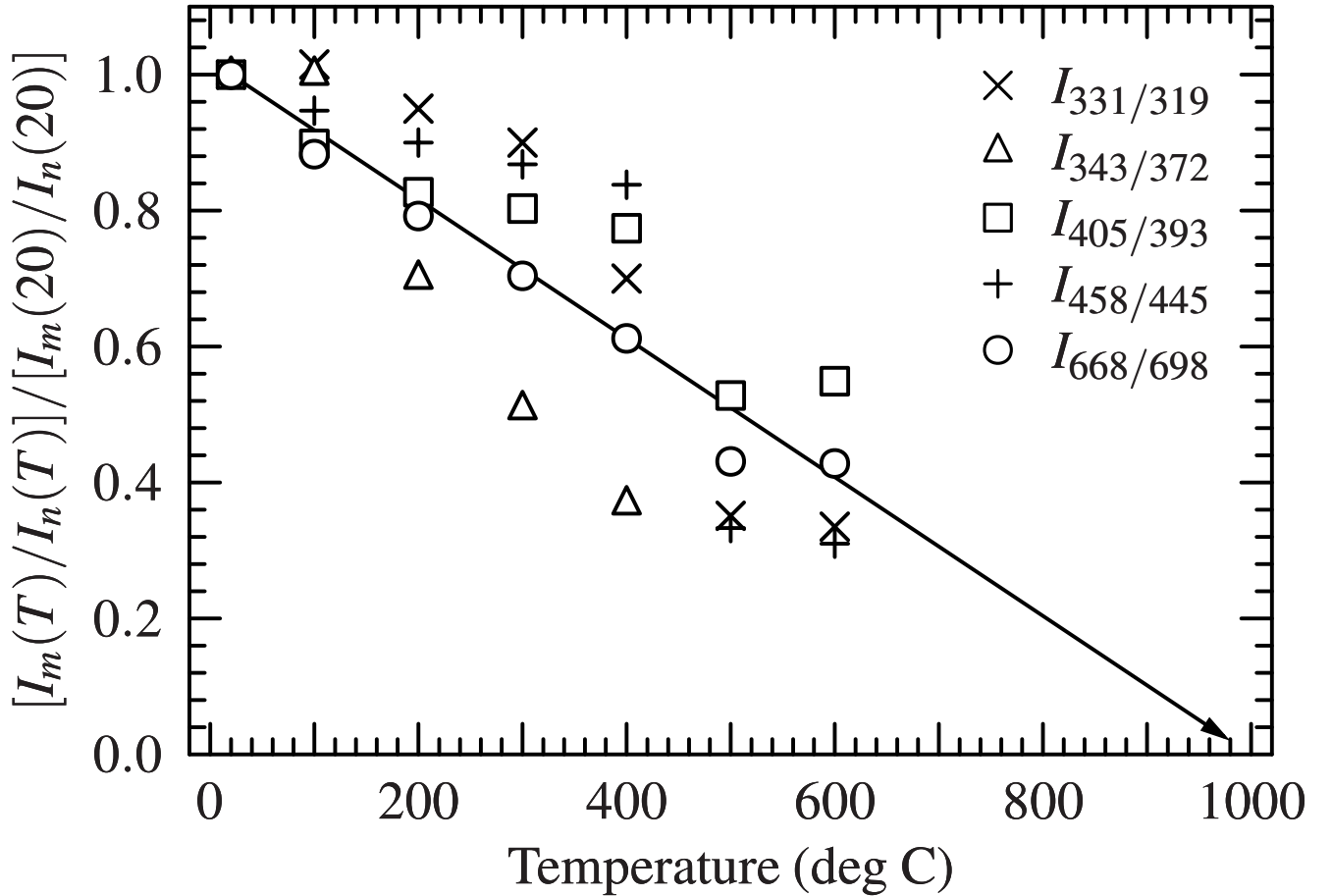

FIG. 6. The temperature dependence of the normalized relative intensity of the five A_g lines vanishing at high temperatures.

In Sc_3CrO_6, due to the same charge of Sc^{3+} and Cr^{3+} ions and relatively close averaged bond length for the two types of CrO_6 and ScO_6 octahedra, we expect that such molecular approach will correctly describe only the modes with highest frequency (internal stretching modes for the CrO_6 octahedra). In Fig. 7 the calculated by LDC frequencies of all fifty-seven optical Γ-point modes are displayed. It is seen that a group of eight modes are placed in the high frequency region (above $550\,\text{cm}^{-1}$). Accounting for their symmetry and their shape (predicted by LDC) we succeed to determine their origin. From the inset of Fig. 7 it can be

concluded that the splitting due to rhombohedrality is smaller than Davydov's splitting. This is expected, because the Davydov's pair of modes actually has different vibrational shape (with very different frequency) for the ScO_6 octahedra.
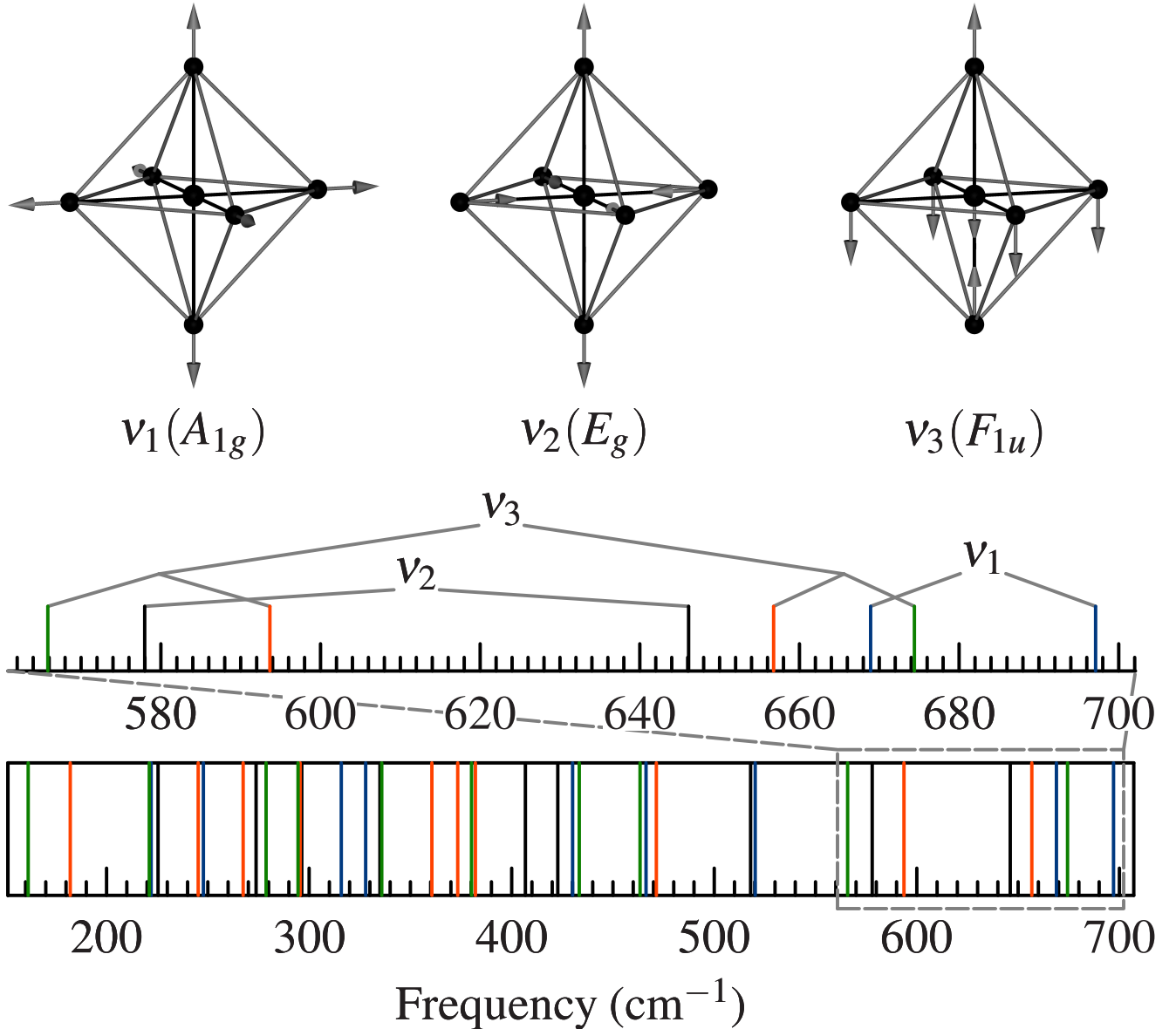

FIG. 7. (Color online) The predicted LDC frequencies of all 57 optical modes in Sc_3CrO_6. A_g, E_g, A_u and E_u modes are displayed with blue, black, green and red ticks. The splitting of the three stretching XY_6 molecular modes, forming the modes with highest frequency in the Sc_3CrO_6, is shown.

Going back to the Fig. 5 we can note that with the increase of the temperature, the crystal stay essentially rhombohedral, because no merge of lines into pairs is observed. However, the decrease of the intensity of five A_g lines can be expected at hypothetical structural phase transition from $R\bar{3}$ to $R\bar{3}c$, where five A_g modes in $R\bar{3}$ become silent A_{2g} modes in $R\bar{3}c$ (see Table V). The LDC predicts that the two high frequency A_g modes experimentally observed at 668 and 698 cm^{-1} originate from v_1 Davydov's pair. The mode with higher frequency is the in-phase vibration of the two octahedra, whereas the mode with lower frequency corresponds to the mode with out-of-phase vibration. The molecular approach predicts that the out-of-phase A_g (v_1) vibration has to be transformed into silent A_{2g} mode in $R\bar{3}c$. Indeed, just the A_g line at 668 cm^{-1} is one of the five lines with decreasing intensity.

IV. CONCLUSIONS

Single crystals of Sc_3CrO_6 were grown and studied using x-ray single crystal diffractometry, scanning electron microscopy with x-ray microprobe analysis and micro-Raman spectroscopy. The chemical content is non-stoichiometric resulting in two different $Cr1O_6$ and $(Cr,Sc)2O_6$ octahedra, in agreement with the refined $R\bar{3}$ crystal structure. From appropriately chosen crystal surfaces, polarized Raman spectra in different geometrical configurations were collected at room temperature and the symmetry of all $9A_g + 9E_g$ Raman-allowed modes was determined. This assignment was confirmed by the results of the performed LDC. A molecular approach for interpretation of the calculated modes was used. It predicts grouping of modes into sets with close frequencies because of two reasons: (a) the presence of two CrO_6 octahedra in the unit cell, and (b) the rhombohedral structure is very close to a cubic one. Indeed, the origin of the eight high frequency modes (corresponding to the internal stretching CrO_6 octahedral vibrations), as it was obtained by LDC, justifies this approach. The changes of the Raman spectra, collected at high temperatures, does not support the rhombohedral-cubic phase transition scenario, but rather suggests a possible transition from $R\bar{3}$ to $R\bar{3}c$ above the investigated temperature region.

ACKNOWLEDGMENTS

---

[*] neno@phys.uni-sofia.bg

[1] S. J. Schneider, R. S. Roth, and J. L. Waring, J. Res. Nat. Bur. Stand. Sect. A **65**, 345 (1961).

[2] W. Sinclair, R. A. Eggleton, and A. E. Ringwood, Z. Kristallogr. **149**, 307 (1979).

[3] J.-H. Park and J. Parise, Mater. Res. Bull. **32**, 1617 (1997).

[4] H. Schulz and G. Bayer, Naturwissenschaften **57**, 393 (1970).

[5] R. Newnham, J. Dorrian, and E. Meagher, Mater. Res. Bull. **5**, 199 (1970).

[6] M. Weil, Acta Crystallogr. Sect. E **62**, i244 (2006).

[7] D. Müller, W. Assenmacher, and W. Mader, Z. Anorg. Allg. Chem. **630**, 2483 (2004).

[8] H. Yusa, T. Tsuchiya, N. Sata, and Y. Ohishi, Inorg. Chem. **48**, 7537 (2009).

[9] J. R. Sahu, C. R. Serrao, and C. N. R. Rao, Solid State Commun. **145**, 52 (2008).

[10] B. Rajeswaran, D. I. Khomskii, A. Sundaresan, and C. N. R. Rao, "Ferroelectricity at the Neel Temperature of Chromium in Rare-earth Orthochromites: Magnetic Jahn-Teller effect," (2012), arXiv:1201.0826v1.

[11] D. Richard, E. L. Muñoz, T. Butz, L. A. Errico, and M. Rentería, Phys. Rev. B **82**, 035206 (2010), and references therein.

[12] A. Lempicki, C. Brecher, P. Szupryczynski, H. Lingertat, V. Nagarkar, S. Tipnis, and S. Miller, Nucl. Instrum. Methods Phys. Res. Sec. A **488**, 579 (2002).

[13] CrysAlisPro, Agilent Technologies UK Ltd., 2010.

[14] G. M. Sheldrick, Acta. Crystallogr. Sect. A **64**, 112 (2008).

[15] Further details of the crystal structure investigation may be obtained from Fachinformationszentrum Karlsruhe, CSD number 424191.

[16] N. D. Todorov, M. V. Abrashev, V. G. Ivanov, G. G. Tsutsumanova, V. Marinova, Y.-Q. Wang, and M. N. Iliev, Phys. Rev. B **83**, 224303 (2011).

[17] J. D. Gale, J. Chem. Soc., Faraday Trans. **93**, 629 (1997).

[18] E. Kroumova, M. I. Aroyo, J. M. Perez-Mato, A. Kirov, C. Capillas, S. Ivantchev, and H. Wondratschek, Phase Transit. **76**, 155 (2003); M. I. Aroyo, A. Kirov, C. Capillas, J. M. Perez-Mato, and H. Wondratschek, Acta. Crystallogr. Sect. A **62**, 115 (2006); M. I. Aroyo, J. M. Perez-Mato, C. Capillas, E. Kroumova, S. Ivantchev, G. Madariaga, A. Kirov, and H. Wondratschek, Z. Kristallogr. **221**, 15 (2006).

[19] G. Blasse and W. Hordijk, J. Solid State Chem. **5**, 395 (1972).

[20] K. Nakamoto, "Infrared and Raman Spectra of Inorganic and Coordination Compounds, Part A: Theory and Applications in Inorganic Chemistry," (John Wiley & Sons, Inc., 2009) Sect. 2.8. Octahedral Molecules, pp. 221–237, 6th ed.

[21] A. S. Davydov, Zh. Eksp. Teor. Fiz. **18**, 210 (1948).

[22] G. N. Zhizhin, B. N. Marvin, and V. F. Shabanov, *The Optical Vibrational Spectra of Crystals* (Nauka, Moscow, 1984) in Russian.